

Crack Growth Strategy in Composites under Static Loading

De Xie^{*}, Zhongyan Qian[†], Dade Huang[‡], and Frank Abdi[§]
Alpha STAR Corporation, Long Beach, CA, 90804

Crack growth in composites can be analyzed by a strategy of two independent steps. The first step, based on the material strength theory, is used to predict the damage mechanism, damage pattern, and the crack growth path. In the second step, fracture mechanics is used to determine the failure loads. The procedure of this strategy is demonstrated by laminated double cantilever beam and fracture coupons (center crack, inclined crack and compact tension) made of stitched warp-knit fabric composites.

I. Introduction

THE crack growth in composites is a complex phenomenon, even under static loading. Currently, two major groups of theories exist in the crack growth analysis for composites: material strength theory and fracture mechanics theory. Each has its own advantages and disadvantages. This paper works towards a strategy to combine the two theories and therefore, it involves an analysis procedure of two steps. Fig. 1 shows the scheme of such strategy with GENOA/PFA, a failure analysis product of Alpha STAR Corporation.

The first analysis, based on the material strength theory, is used to determine the damage mechanism, damage pattern and the crack path. In this analysis, the failures such as fiber breaking, fiber kinking, matrix cracking, and fiber/matrix interface debonding can be detected based on different failure criteria (stress, strain, or the combination of stress and strain such as distortion energy). The advantage of this approach is that it does not require the predefined crack path. However, in the case of removing the damaged elements can create the stress singularity. Therefore, a second analysis is performed based on the fracture mechanics theory to improve the prediction capability for the failure loads.

In the second analysis, the node pairs are embedded along the crack path that was determined from the first analysis. A cohesive zone model (CZM) was used to account for the processing zone at the crack tip due to micro cracking, fiber bridging, coalescence of voids and other resources of micro level interactions in composites. DCZM (discrete cohesive zone model) is a numerical approach to implement

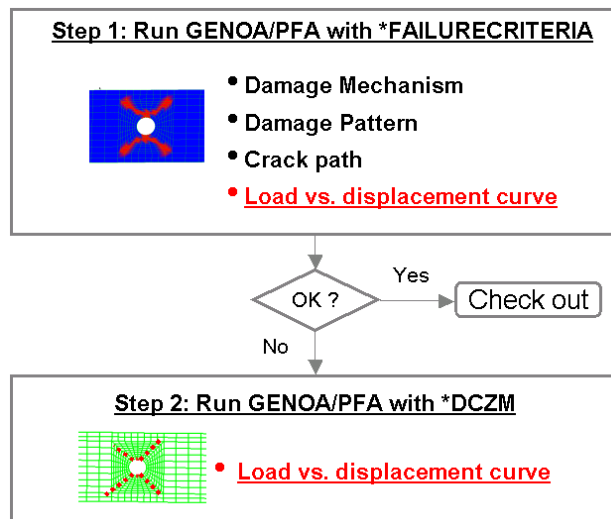


Figure 1. Scheme of crack growth strategy in composite under static loading with GENOA/PFA

^{*} Structure Engineer, dxie@alphastarcop.com, AIAA Member.

[†] Engineer, jqian@alphastarcop.com, AIAA Member.

[‡] Director of Software Development, huangd@alphastarcop.com, AIAA Member.

[§] CEO, fabdi@alphastarcop.com, AIAA Member.

CZM in conjunction with finite element analysis (FEA) and is used to control the crack growth. The advantages of DCZM are its insensitivity to the FEA mesh size and its capability of modeling material softening without severe convergence difficulties.

To illustrate this two-steps analysis strategy, this paper begins with a laminated double cantilever beam (DCB) example. The crack propagation path is determined by the modified distortion energy (MDE) criteria. Then, DCZM was used to predict the load vs. deflection curve. Different values for the cohesive strength may generate very different load vs. displacement curves, for both the peak load and the curve shape. To determine the unique curve cohesive strength, calibration is required. This calibration procedure was then illustrated by analyzing four fracture specimens made of stitched warp-knit fabric. The calibration from a narrow central crack panel (CC2) determines the cohesive strength is 65% of the tensile strength measured from regular tensile coupons. With this value for the cohesive strength, the DCZM was applied to other specimens such as the wide central crack panel (CC4), the inclined central crack panel (IC) and the compact tension (CT). The relative errors for the predicted maximum load by DCZM are -3%, -2% and -3% compared to the corresponding test data for CC4, IC and CT, respectively. Also, DCZM successfully captures the nonlinear features that were observed in the test curves. In summary, the first analysis based on material strength is qualitative while the second analysis based on fracture mechanics is quantitative. This two-steps analysis strategy could be a practical tool for engineers to investigate crack growth problems in composite structures.

II. Summary of Formulations

A. Interactive Strength based Failure Criteria ^[1-5]

Progressive failures are detected by failure criteria locally at laminar ply level. The first set of twelve failure modes is directly associated with the positive and negative limits of the six local stress components in the material direction. For normal stress, the three criteria are:

$$S_{I11C} < \sigma_{I11} < S_{I11T}, \quad S_{I22C} < \sigma_{I22} < S_{I22T}, \quad \text{and} \quad S_{I33C} < \sigma_{I33} < S_{I33T} \quad (1)$$

where the subscripts “*T*”, “*C*” and “*T*” refer to layer, compression and tension, respectively. “*S*” represents material strength. Six values of normal strength are required as inputs. These values can be measured from standard coupon tests. “ σ ” represents stress state that is computed in a finite element analysis. For shear stress, the three criteria are

$$-S_{I12} < \sigma_{I12} < S_{I12}, \quad -S_{I23} < \sigma_{I23} < S_{I23}, \quad \text{and} \quad -S_{I13} < \sigma_{I13} < S_{I13} \quad (2)$$

Three values of shear strength are required as inputs.

The second set has one failure mode that is determined by a combined stress failure criterion, or modified distortion energy (MDE) failure criterion:

$$\left(\frac{\sigma_{I11\alpha}}{S_{I11\alpha}} \right)^2 + \left(\frac{\sigma_{I22\beta}}{S_{I22\beta}} \right)^2 - K_{I12\alpha\beta} \frac{\sigma_{I11\alpha}}{S_{I11\alpha}} \frac{\sigma_{I22\beta}}{S_{I22\beta}} + \left(\frac{\sigma_{I12S}}{S_{I12S}} \right)^2 < 1 \quad (3)$$

where α and β indicate tensile or compressive stresses, $S_{I11\alpha}$ is the local longitudinal strength in tension or compression, $S_{I22\alpha}$ is the transverse strength in tension or compression, and the directional interaction factor is defined as:

$$K_{I12\alpha\beta} = K'_{I12\alpha\beta} \frac{(1+4\nu_{12}-\nu_{13})E_{22} + (1-\nu_{23})E_{11}}{\sqrt{E_{11}E_{22}(2+\nu_{12}+\nu_{13})(2+\nu_{21}+\nu_{23})}} \quad (4)$$

where $K'_{I12\alpha\beta}$ is a theory-experiment correlation factor.

B. Discrete Cohesive Zone Model (DCZM) ^[6-20]

In fracture mechanics, strain energy release rate (G) is one of the fracture parameters that are used increasingly. VCCT (virtual crack closure technique) is a numerical method that was introduced to compute G in conjunction with FEA [6-7]. Then G is compared against the fracture toughness of a coupon to predict the crack growth. This

method requires a sharp crack tip of elastic material with small yielding zone around the crack tip. When material non-linearity at the crack tip is negligible, this technique has been proven to be effective in predicting crack initiation and the subsequent growth.

However, for composites, the material non-linearity at the crack tip cannot be neglected. For composites, there exists a processing zone ahead of crack tip due to micro cracking, fiber bridging, coalescence of voids and other resources of micro level interactions. This processing zone makes the crack tip blunt and thus invalids the VCCT. CZM was introduced to account for this damage zone (or material softening) that develops near the crack tip. The crack is initiated when the stress attains the cohesive strength and the crack front is advanced gradually as the fracture energy is exhausted [8].

CZM can be implemented with FEA by using continuum type elements when the CZM is considered as a *continuous compliant layer* [9-13, 20]. Another version for implementation is to treat the CZM as a *discrete spring foundation* [14-19]. In this case, spring type elements are used to accommodate the model. We refer to the first type as CCZM (continuum cohesive zone model) and the second type as DCZM (discrete cohesive zone model). In this paper, DCZM is used. The current DCZM applies the cohesive law to the spring force vs. displacement separation and has advantages such as (1) no element aspect ratio trouble since the spring can be zero elongation; (2) The cohesive strength can be scaled to the nodal force to avoid the severe mesh dependency.

For a crack line in the global space (X, Y, Z) with crack tip at nodal pair (1,2), see Fig. 2, the effective cohesive zone size is

$$\Delta a = \sqrt{(X_5 - X_3)^2 + (Y_5 - Y_3)^2 + (Z_5 - Z_3)^2} / 2 \quad (5)$$

where, (X_3, Y_3, Z_3) and (X_5, Y_5, Z_5) are the global coordinates for nodes 3 and 5 shown in Figure 2. The crack tip opening Δu , Δv and Δw are computed between nodes 1 and 2 in the global coordinate system and projected into the local coordinate system to obtain δ_1 , δ_2 and δ_3 , corresponding to mode I, mode II and mode III, respectively. Same procedure is applied to the local nodal forces F_1 , F_2 , and F_3 at the crack tip.

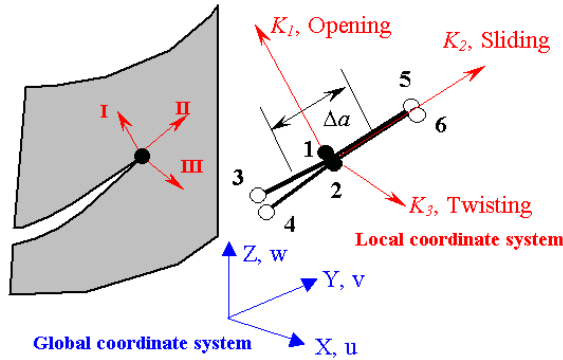


Figure 2. Definitions of the local coordinate system

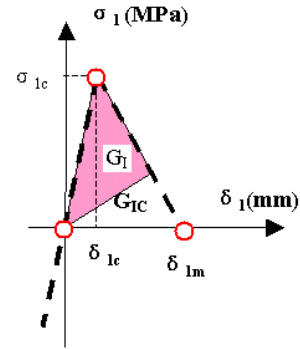


Figure 3. Triangle type cohesive law

For the triangle type cohesive law shown in Fig. 3 and the mode I fracture, the cohesive nodal force (F_{1c}) is calculated based on the cohesive strength (σ_{1c}), body thickness at crack tip (B) and cohesive size (Δa):

$$F_{1c} = \sigma_{1c} B \Delta a \quad (6)$$

In equation (6), the nodal force F_{1c} is scaled to the FEA size by Δa to eliminate the FEA mesh dependency. The critical opening at the crack tip is

$$\delta_{1c} = \frac{F_{1c}}{K_1} \quad (7)$$

Where, K_I is the cohesive stiffness for mode I. Refer to the triangle cohesive law shown in Fig. 2, the energy required to fracture is the area covered by the triangle. Based on this, the maximum separation (δ_{1m}) is

$$\frac{1}{2}\sigma_{1c}\delta_{1m} = G_{IC} \quad (8)$$

Or, equivalently,

$$\delta_{1m} = \frac{2G_{IC}}{\sigma_{1c}} \quad (9)$$

Where G_{IC} is the mode I fracture toughness.

Now the triangle to represent the cohesive law is determined. Next, we apply the cohesive zone law

$$\text{If } \delta_{1c} < \delta_1 < \delta_{1m} : K_I = \left(\frac{\delta_{1m}}{\delta_1} - 1.0 \right) \frac{F_{1c}}{\delta_{1m} - \delta_{1c}} \text{ and } G_I = \frac{\delta_1 - \delta_{1c}}{\delta_{1m} - \delta_{1c}} G_{IC} \quad (10a)$$

$$\text{If } \delta_1 > \delta_{1m} : K_I = 0.0 \text{ and } G_I = G_{IC} \quad (10b)$$

For the mixed mode fracture, same procedure is applied to Mode II (sliding) and Mode III (twisting). Once the following criteria is satisfied,

$$\frac{G_I}{G_{IC}} + \frac{G_{II}}{G_{IIC}} + \frac{G_{III}}{G_{IIIC}} \geq 1.0 \quad (11)$$

release all the spring in all the directions between nodes 1 and 2 and then the crack tip advances.

III. Results and Discussions

Two examples are used to illustrate the strategy. First, a laminated double cantilever beam is analyzed. The mesh sensitivity of mesh size and the effect of the cohesive strength are investigated. Next, four fracture specimens made of stitched warp-knit fabric are studied to demonstrate the calibration procedure for cohesive strength.

A. Double Cantilever Beam Made of Laminate ^[20]

A double cantilever beam (DCB) of laminated composites was studied first. Alfano and Crisfield have studied the same problem with VCCT and CCZM [20]. As a pure mode I problem, the DCB was loaded by displacement control. The geometry is described in Fig. 4. The laminate properties in analysis are: $E_{11}=135.3\text{GPa}$; $E_{22}=9.0\text{GPa}$; $G_{12}=5.2\text{GPa}$; $\nu_{12}=0.24$ and fracture toughness for mode I is $G_{IC}=0.28 \text{ N/mm}$ [20].

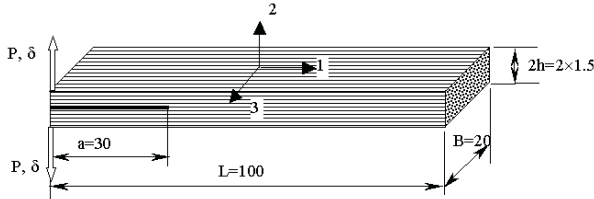


Figure 4. Dimensions of DCB



Figure 5. Crack path predicted by GENOA/PFA with Failure Criteria

First, run GENOA/PFA without DCZM [21]. The GENOA/PFA predicts that the crack grows along the initial crack line, shown in Fig. 5. Next, the DCZM is applied along the crack path shown in Fig. 5. Figs 6 to 8 show the results of different case studies. The VCCT results by Crisfield and by GENOA/PFA are also shown as references.

Figure 6 studies the displacement increment sensitivity. In this case, a 400 elements FEA model was used. The cohesive strength is chosen as $\sigma_{1c}=0.285\text{MPa}$ and cohesive stiffness (K_I) is $200 \cdot 10^4 \text{ N/mm}$. Four different

displacement increments (0.2mm, 0.1mm, 0.05mm, 0.01mm) were studied. One can see that the result from 0.2mm increment significantly differs from the others. However, as the displacement increment becomes fine, the results are converged. As a result, the load vs. displacement curves of 0.01mm and 0.05 mm are almost the same. For this case, increment of 0.1mm can generate very good results.

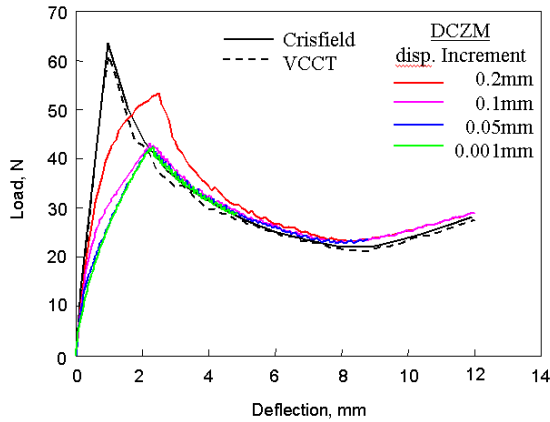


Figure 6. Displacement Increment study

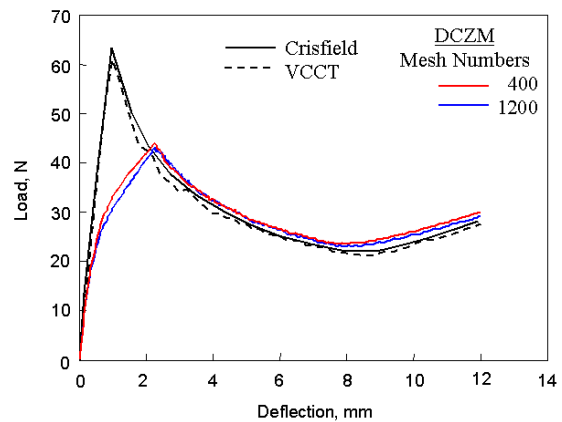


Figure 7. Mesh sensitivity study

Figure 7 shows the load vs. displacement curves from two mesh sizes: 400 and 1200 elements, respectively. In this study, the displacement increment is 0.1mm. The cohesive strength is chosen as $\sigma_{1C}=0.285\text{MPa}$ and cohesive stiffness (K_I) is $200 \cdot 10^4 \text{ N/mm}$. From Fig. 7, one can see that the present DCZM is not sensitive to the mesh size once a reasonably dense mesh is used.

Figure 8 shows the load vs. displacement curves from a series of cohesive strength. In this case, mesh 400 is used and the displacement increment is 0.1mm. The cohesive stiffness (K_I) is $200 \cdot 10^4 \text{ N/mm}$. As the cohesive strength increases, the maximum load increases. For lower cohesive strength, the shape of the curves differs from that of VCCT, which VCCT assumes the linear elastic type material. The cohesive strength needs to be calibrated from coupons based on both the curve shape and the maximum load to account for the material nonlinearity.

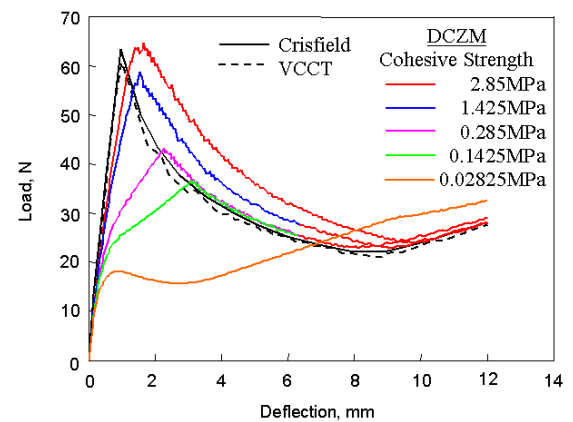


Figure 8. Cohesive strength study

B. Fracture Coupons Made of Stitched Warp-Knit Fabric ^[22]

McDonnell Douglas (now Boeing) will design and build an all-composite wing for a commercial transport aircraft as a part of NASA's AST Composite Wing Program. This requires that the wing maintain adequate strength after sustaining detectable impact damage and discrete source damage. AS4 carbon warp-knit fabric, using technologies adapted from textile industry, is among candidate composites. Therefore, a series of tests was conducted to measure the fracture toughness of such composites.

Three types of test specimens were evaluated: central crack (CC), inclined crack (IC), and compact tension (CT). For CC, two specimens were tested: one is 2.0 inch wide (CC2) and the other is 4.0 inch wide (CC4). Table 1 summarizes the data for crack length of each case.

The composite contains AS4 fibers in 0° , $\pm 45^\circ$ and 90° directions. By area weight, 44% of the fibers were configured in the 0° direction,

Table 1. Summary of crack length

Symbol	Notation	W (in.)	2a/w	2a (in.)	a/w	a (in.)
CC2	501-CN2	2.0	0.25	0.5	N/A	N/A
CC4	501-CN1L	4.0	0.25	1.0	N/A	N/A
IC	501-ICN1	2.0	0.25*	0.5*	N/A	N/A
CT	501-CT-21	1.4	N/A	N/A	0.5	0.7

* These values refer to the projected crack length for the inclined cracks

44% in the $\pm 45^\circ$ directions, and 12% in the 90° direction (page 2 of [22]). Based on this, the thickness of each lamina can be estimated. The elastic constants for the material are: $E_1=10.4\text{Msi}$, $E_2=5.22\text{Msi}$, $\nu_{xy}=0.403$, and $\nu_{yz}=0.202$ (page 4 of [22]). The average value of tensile strength from coupon tests is 119.2ksi . (Table II of [22]).

Table 2 summarizes the data for fracture toughness of each type of specimens. The critical values for stress intensity factors (K_{I0} and $K_{I\max}$) are measured from tests. The critical values for strain energy release rates (G_{I0} and $G_{I\max}$), which will be used as inputs for DCZM analysis, are estimated by

$$G = \frac{K^2}{E_1} \quad (12)$$

The CC2 is chosen for the calibration of the cohesive strength. Fig. 9(c) shows the stress vs. COD (crack opening displacement) curves from test (thick solid black line), VCCT (thick dashed black line) and DCZM (thin lines with different colors). For VCCT, the predicted maximum stress is 52.5ksi , which is 81% of the test data (64.5ksi). The relative error is -19% . The stress vs. COD curve predicted by VCCT is sudden load drop immediately after the maximum stress. It does not capture the nonlinear portion of the test curve. The DCZM

Table 2. Summary of fracture toughness

Notation	Notation in Ref [22]	ksi-in ^{1/2}		lb/in	
		K_{I0}	$K_{I\max}$	G_{I0}	$G_{I\max}$
CC2	501-CN2	N/A	60.9	N/A	356.6
CC4	501-CN1L	N/A	77.2	N/A	573.1
IC	501-ICN1	N/A	57.8	N/A	321.2
CT	501-CT-21	44.1	53.6	187.0	276.2

successfully captured this feature. Different cohesive strength values, 100%, 70%, 65% and 50% of the tensile strength (119.2ksi) are run to perform the calibration. For 65% cases, where cohesive strength is 77.48ksi , the predicted maximum stress is 64.6ksi . The relative error is $+0.2\%$. This accuracy is sufficient. Therefore, we consider the value of 77.48ksi as the cohesive strength of this material and apply it for other cases.

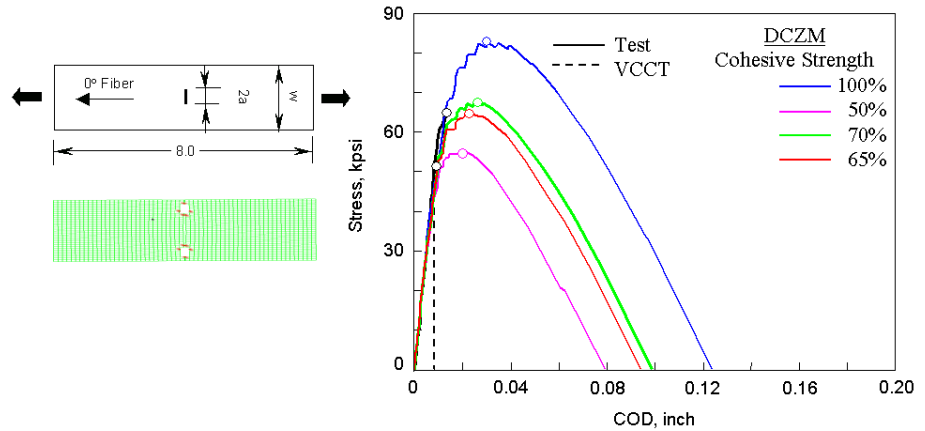


Figure 9. CC2 is used for calibration

First application example is CC4, which is an enlarged CC2. Figure 10 shows the stress vs. COD curves from test (thick solid black line), VCCT (thick dashed black line) and DCZM (thin red line). Again, VCCT predicted a sudden load drop that differs from the test. The predicted maximum stress is 49.5ksi . The test data is 58.8ksi . The relative error is -16% .

VCCT is only valid for elastic materials. It is not a surprise to see a large discrepancy since the current material shows significant nonlinear behavior. For DCZM, it successfully captured the nonlinear feature. The predicted maximum stress is 57.6ksi which has the relative error of -2.7% . The DCZM prediction agrees well with the test.

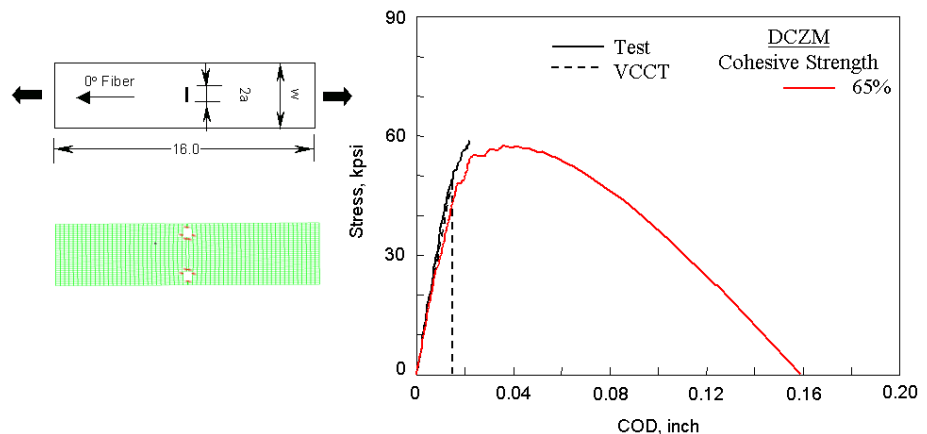


Figure 10. Comparisons between test and predictions for CC4

Figure 11 shows the stress vs. COD curves predicted by VCCT and DCZM for the IC. In this case, the test data is not available in Ref [22]. The measured maximum stress is 61.3ksi. The VCCT predicts the maximum stress of 45.0ksi. The relative error is -26%. The DCZM predicts the maximum stress of 60.0ksi and relative error is -2.1%. The DCZM result agrees with the test data very well.

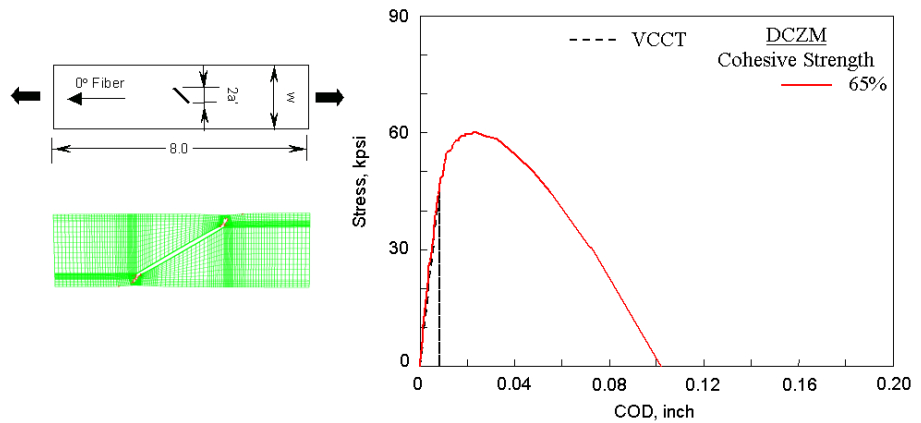


Figure 11. predictions for IC

Finally, the DCZM is applied to CT. Figure 12 presents the load vs. COD curves from test (thick black line), VCCT (thick blue line) and DCZM (thin red line). The load vs. COD has a different feature this case due to different configuration of CT than the other three (CC2, CC4 and IC). The VCCT predicts the maximum load of 1.44 kips. The measured maximum load is 2.31kips. The relative error is -37%. The DCZM prediction for this value is 2.21kips. The relative error is -3%. DCZM captures the feature of the load vs. COD curve.

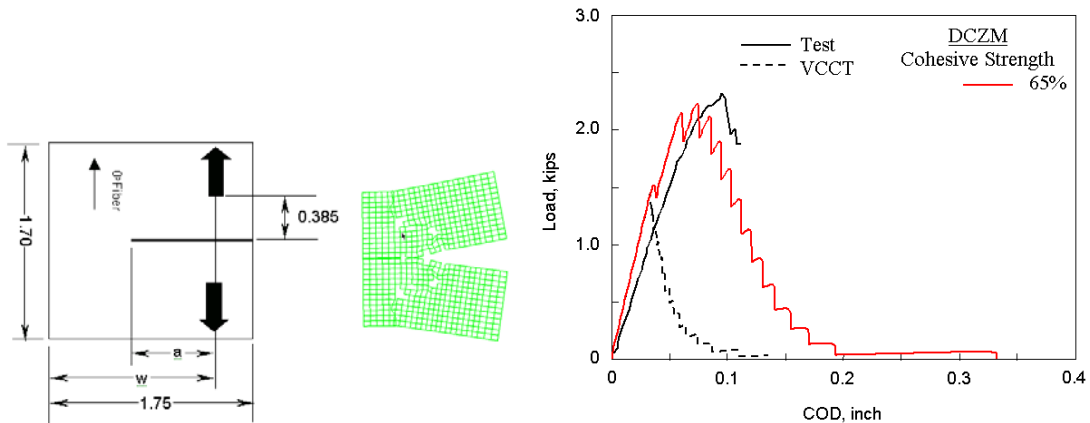


Figure 12. Comparisons between test and predictions for CT

IV. Conclusion

A two-steps analysis strategy was introduced to deal with the crack growth problems under static loading. In the first analysis, the damage mechanism, damage pattern, and the crack path were obtained. In the second analysis, discrete cohesive zone model (DCZM) was used to control the crack growth. The procedure was demonstrated by two examples: DCB of laminate and fracture coupons of stitched warp-knit fabric. The calibration process was illustrated. This two-steps analysis strategy could be a practical tool for engineers to investigate crack growth problems in composite structures.

References

1. Hill, R., *The Mathematical Theory of Plasticity*, Oxford University Press, Oxford, 1950.
2. Tsai, S.W., "Strength Theories of Filamentary Structures," Chapter 1 in *Fundamental Aspects of Fiber Reinforced Plastic Composites* (Schwartz, R.T., and Schwartz, H.S. Eds.), Interscience, New York, 1968.

3. Chamis CC, "Failure Criteria for Filamentary Composites," Composite Materials Testing and Design: ASTM STP 460, American Society for Testing and Materials, Philadelphia, 1969, pp 336-351.
4. Huang, D., Abdi, F., and Khatiblou, M., "Progressive Failure Analysis (PFA) and Verification of Composite Test Panel under Impact and Tension after Impact (TAI) Loading Using GENOA," Alpha STAR Technical Report to Boeing, 1999.
5. Huang, D., Abdi, F., and Khatiblou, M., "Progressive Failure Analysis (PFA) and Verification of Composite Test Panel under Impact and Compression after Impact (CAI) Loading Using GENOA," Alpha STAR Technical Report to Boeing, 1999.
6. Xie, D., and Biggers Jr., S.B., "Strain Energy Release Rate Calculation for a Moving Delamination Front of Arbitrary Shape based on Virtual Crack Closure Technique, Part I: Formulation and validation," *Engineering Fracture Mechanics*, Vol. 73, No. 6, 2006, pp. 771-785.
7. Xie, D., and Biggers Jr., S.B., "Strain Energy Release Rate Calculation for a Moving Delamination Front of Arbitrary Shape based on Virtual Crack Closure Technique, Part II: Sensitivity Study on Modeling Details," *Engineering Fracture Mechanics*, Vol. 73, No. 6, 2006, pp. 786-801.
8. Ungsuwarungsri, T., and Knauss, W.G., "The Role of Damage-Softened Material Behavior in the Fracture of Composites and Adhesives," *International Journal of Fracture*, Vol. 35, No. 3, 1987, pp. 221-241. See also Ph.D. thesis, 1985, Aeronautics Department, Caltech, Pasadena, CA.
9. Davila, C.G., Camanho, P.P., de Moura, M.F., "Mixed-mode Decohesion Elements for Analyses of Progressive Delamination," *42nd AIAA/ASME/ASCE/AHS/ASC Structures, Structural Dynamics & Materials Conference*, AIAA-2001-1486, Seattle, WA. April 16-19, 2001.
10. Camanho, P.P., Davila, C.G., and Ambur, D.R., "Numerical Simulation of Delamination Growth in Composite Materials", NASA/TP-2001-211041, 2001.
11. Goyal, V.K., Johnson, E.R., Dávila, C.G., and Jaunky, N., "An Irreversible Constitutive Law for Modeling the Delamination Process Using Interface Elements," *43rd AIAA/ASME/ASCE/AHS/ASC Structures, Structural Dynamics & Materials Conference*, AIAA-2002-15766, Denver, CO. April 22-25, 2002.
12. Camanho, P.P., Davila, C.G., and de Moura, M.F., "Numerical Simulation of Mixed-mode Progressive Crack in Composite Materials," *Journal of Composite Materials*, Vol. 37, No. 16, 2003, pp. 1415-1438.
13. Turon, A., Davika, C.G., Camanho, P.P., and Costa, J., "An Engineering Solution for Using Coarse Meshes in the Simulation of Delamination with Cohesive Zone Model," NASA/TM-2005-213547, 2005.
14. Song, S.J., and Waas, A.M., "A Spring Foundation Model for Mode-I Failure of Laminated Composites based on an Energy Criterion," *Journal of Engineering Materials and Technology*, Vol. 116, No. 4, 1994, pp. 512-516.
15. Song, S.J., and Waas, A.M., "Energy-based Mechanical Model for Mixed-mode Failure of Laminated Composites," *AIAA Journal*, Vol. 33, No. 4, 1995, pp. 739-745.
16. Shahwan, K.W., and Waas, A.M., "Non-self-similar Decohesion along a Finite Interface of Unilaterally Constrained Delaminations," *Proceedings of the Royal Society of London. Series A: Mathematical and physical sciences*, Vol. 453, No. 1958, 1997, pp. 515-550.
17. Xie, D., Salvi, A.G., Waas, A.M., and Caliskan, A., "Discrete Cohesive Zone Model to Study Static Fracture in a Plate of Textile Braided Carbon Fiber Composites," *46th AIAA/ASME/ASCE/AHS/ASC Structures, Structural Dynamics & Materials Conference*, AIAA-2005-2320, Austin, TX, April 18-21, 2005.
18. Xie, D., Salvi, A.G., Sun, C., Waas, A.M., and Caliskan, A., "Discrete Cohesive Zone Model to Study Static Fracture in a Plate of Textile Braided Carbon Fiber Composites," *Journal of Composite Materials*, in press.
19. Xie, D., and Waas, A.M., "Discrete Cohesive Zone Model for Mixed-Mode Fracture using Finite Element Analysis," *Engineering Fracture Mechanics*, in press.
20. Alfano, G., and Crisfield, M.A., "Finite Element Interface Models for the De-lamination Analysis of Laminated Composites: Mechanical and Computational Issues," *International Journal for Numerical Methods in Engineering*, Vol. 50, No. 7, 2001, pp. 1701-1736.
21. "GENOA Fracture Toughness Simulation of Un-Reinforced Double Cantilever Beam (DCB) Test Specimen," Technical Report, Alpha STAR Corporation, 1999.
22. Masters, J.E., "Translaminar Fracture Toughness of a Composite Wing Skin Made of Stitched Warp-knit Fabric," NASA Contractor Report 201728, 1997.